JACS
JOURNAL OF THE AMERICAN CHEMICAL SOCIETY
Communication
Cite This: J. Am. Chem. Soc. 2019, 141, 19988−19993
pubs.acs.org/JACS

NMR Chemical Exchange Measurements Reveal That N^6-Methyladenosine Slows RNA Annealing

Honglue Shi,[†,⊥] Bei Liu,[‡,⊥] Felix Nussbaumer,[§] Atul Rangadurai,[‡] Christoph Kreutz,*[,§] and Hashim M. Al-Hashimi*[,†,‡]

[†]Department of Chemistry, Duke University, Durham, North Carolina 27710, United States
[‡]Department of Biochemistry, Duke University School of Medicine, Durham, North Carolina 27710, United States
[§]Institute of Organic Chemistry and Center for Molecular Biosciences Innsbruck (CMBI), University of Innsbruck, 6020 Innsbruck, Austria

Supporting Information

ABSTRACT: N^6-Methyladenosine (m^6A) is an abundant epitranscriptomic modification that plays important roles in many aspects of RNA metabolism. While m^6A is thought to mainly function by recruiting reader proteins to specific RNA sites, the modification can also reshape RNA-protein and RNA−RNA interactions by altering RNA structure mainly by destabilizing base pairing. Little is known about how m^6A and other epitranscriptomic modifications might affect the kinetic rates of RNA folding and other conformational transitions that are also important for cellular activity. Here, we used NMR $R_{1\rho}$ relaxation dispersion and chemical exchange saturation transfer to noninvasively and site-specifically measure nucleic acid hybridization kinetics. The methodology was validated on two DNA duplexes and then applied to examine how a single m^6A alters the hybridization kinetics in two RNA duplexes. The results show that m^6A minimally impacts the rate constant for duplex dissociation, changing k_{off} by ∼1-fold but significantly slows the rate of duplex annealing, decreasing k_{on} by ∼7-fold. A reduction in the annealing rate was observed robustly for two different sequence contexts at different temperatures, both in the presence and absence of Mg^{2+}. We propose that rotation of the N^6-methyl group from the preferred *syn* conformation in the unpaired nucleotide to the energetically disfavored *anti* conformation required for Watson−Crick pairing is responsible for the reduced annealing rate. The results help explain why in mRNA m^6A slows down tRNA selection and more generally suggest that m^6A may exert cellular functions by reshaping the kinetics of RNA conformational transitions.

N^6-Methyladenosine (m^6A) is an abundant reversible epitranscriptomic modification found in coding and noncoding RNAs.[1−4] It plays important roles in RNA metabolism[5−8] and is implicated in a growing number of cellular processes.[9−15] While the modification is thought to primarily exert its function by recruiting reader proteins to specific RNA sites, it can also reshape RNA−RNA and RNA-protein interactions by modulating RNA structure.[16−20] A single m^6A destabilizes RNA duplexes by 0.5−1.7 kcal/mol,[21,22] enhancing binding to single-stranded RNA (ssRNA) binding proteins.[16] m^6A destabilizes A-U base pairs (bps) because hydrogen bonding requires that the N^6-methyl group adopts the energetically unfavorable *anti* conformation[21,22] (Figure 1).

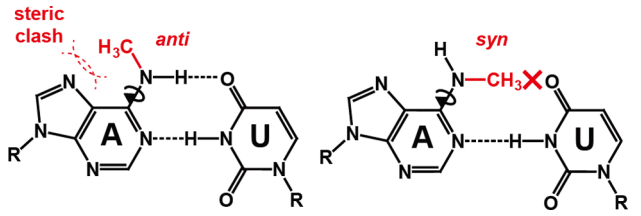

Figure 1. N^6-Methyladenosine (m^6A) destabilizes m^6A-U pairing and RNA duplexes. The methyl group has to adopt an *anti* conformation to form the Watson−Crick H6---O4 hydrogen bond, but this leads to unfavorable steric contacts with N7.

The activities of many RNAs also depend on the kinetic rates of folding, protein-RNA, RNA−RNA, and RNA-ligand association/dissociation, and conformational transitions.[23−29] Surprisingly little is known about how m^6A and other epitranscriptomic modifications impact these kinetic properties of RNA. Compelling evidence for such a kinetic effect comes from a study showing that in mRNA m^6A slows down tRNA selection during translation.[20] Here, we developed an approach based on NMR spin relaxation dispersion (RD) in the rotating frame ($R_{1\rho}$)[30−32] and Chemical Exchange Saturation Transfer (CEST)[33,34] to site-specifically and noninvasively measure hybridization kinetics of nucleic acid duplexes and then used the approach to examine how a single m^6A impacts RNA duplex hybridization kinetics.

The melting and annealing of RNAs occurs in a wide variety of biochemical reactions.[27,35] Relative to other methods for studying hybridization kinetics,[36−45] the NMR approach does not require a potentially perturbing label, which could obscure the impact of a small chemical modification, and kinetics can be measured at atomic resolution[32,46] to enable characterization of any intermediates that may form at the modified site.

Received: October 10, 2019
Published: December 12, 2019

DOI: 10.1021/jacs.9b10939
J. Am. Chem. Soc. 2019, 141, 19988−19993

We first evaluated the $R_{1\rho}$ RD methodology on DNA duplexes whose hybridization kinetics has been extensively characterized previously.[38,41,44,45,47−51] $R_{1\rho}$ RD relies on measuring the exchange contribution (R_{ex}) to transverse spin relaxation (R_2) due to chemical exchange between a major ground-state (GS) and a low-abundance and short-lived "excited-state" (ES).[52,53]

Prior $R_{1\rho}$ studies on RNA and DNA duplexes were carried out at temperatures below the melting temperature (T_m).[46,54−56] Under these conditions, the population (p_{ss}) of the single-stranded (ss) species falls below detection (<0.1%),[31] enabling studies of bp dynamics. For example, at T = 25 °C, the $R_{1\rho}$ profiles measured for various sites in the A_6-DNA duplex[55,57] (T_m ∼ 51 °C and [A_6-DNA] ∼ 0.9 mM) reflect exchange between a major Watson−Crick GS and minor Hoogsteen ES[55] (Figures 2A, 2B, S1). There is no evidence for a transient ss species, which is estimated to have a p_{ss} ∼ 0.1% based on UV melting experiments (Table S1).

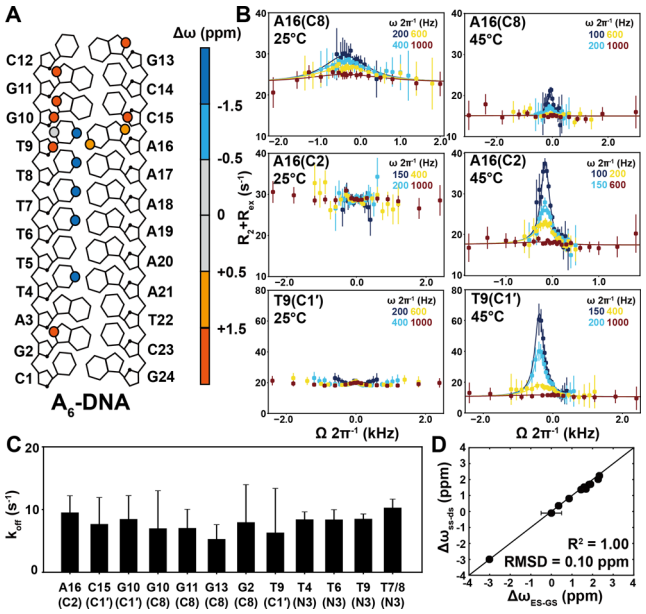

Figure 2. Site-specific characterization of A_6-DNA hybridization kinetics using NMR $R_{1\rho}$ RD. (A) The A_6-DNA duplex. $\Delta\omega = \omega_{ES} - \omega_{GS}$ obtained from global fitting of the $R_{1\rho}$ RD profiles is color-coded on each atom. Sites which are not colored indicate that no measurements were done. (B) Off-resonance $R_{1\rho}$ (^{13}C) RD profiles measured in A_6-DNA at 25 °C (left) and 45 °C (right). T9(C1′) RD at 25 °C was reprinted with permission from 58. Copyright 2018 Springer. Buffer conditions were 25 mM NaCl, 15 mM sodium phosphate, 0.1 mM EDTA, and 10% D_2O at pH 6.8. (C) The site-specific k_{off} values obtained from two-state fitting of the $R_{1\rho}$ RD profiles measured for A_6-DNA at 45 °C. (D) Comparison of $\Delta\omega_{ES\text{-}GS} = \omega_{ES} - \omega_{GS}$ measured by RD with $\Delta\omega_{ss\text{-}ds} = \omega_{ss} - \omega_{ds}$ values obtained from the major and minor resonance observed in 2D [^{13}C,^{1}H], [^{15}N,^{1}H], and [^{15}N, ^{13}C] HSQC spectra of A_6-DNA at 45 °C.

Based on simulations,[50] increasing the temperature so that p_{ss} > 1.0% should bring hybridization kinetics within $R_{1\rho}$ detection (Figure S2). Indeed, the $R_{1\rho}$ profiles for A_6-DNA changed when increasing the temperature to T = 45 °C (p_{ss}∼10%). RD is now apparent at A16(C2) and T9(C1′), which are otherwise flat at T = 25 °C (Figure 2B). A single peak was observed in all cases consistent with two-state exchange (GS ⇌ ES). Fitting the $R_{1\rho}$ data to a two-state exchange model yielded very similar $k_1 = k_{off}$ (differences <2-fold; k_{off} is the rate constant for dissociation) for different sites as expected for concerted melting and annealing of the duplex (Figure 2C). This is in stark contrast to Hoogsteen exchange at T = 25 °C, in which k_1 varies 50-fold across sites reflecting sequence-specific differences in bp dynamics.[59] The ES chemical shifts measured for various sites were also in excellent agreement with those measured for the isolated ss, confirming that the ES is the ss species (Figures 2D, S3).

In the "zip-up" model,[48,60] DNA annealing proceeds through a slow nucleation step followed by a fast zipping step occurring on the ns-μs time scale which is too fast for RD detection. Since the Hoogsteen exchange at higher temperatures is likely too fast for RD detection, "all-or-nothing" behavior is observed with strands either being fully annealed or fully unzipped. These results establish the utility of $R_{1\rho}$ RD to measure hybridization kinetics in DNA duplexes with site-specific resolution.

The backward rate constant $k_{-1} = k_{on} \times$ [ss] (k_{on} is the rate constant for duplex annealing) was ill-defined when fitting the $R_{1\rho}$ RD data (Figure S4). Such a degeneracy is expected when the exchange is slow on the NMR time scale and when using spin lock powers (ω_1) in the $R_{1\rho}$ experiment that exceed the exchange rate ($k_{ex} = k_1 + k_{-1}$).[61,62] Indeed, in the slow exchange limit, the line broadening of the GS resonance only depends on the forward rate. To address this degeneracy, we used CEST experiments which can employ much lower spin locking fields more suitable for characterizing systems in slow exchange.[33,34] CEST relies on measuring the resonance intensity of the GS as a function of the power and offset of an applied weak radio frequency (rf) field. At T = 45 °C, the CEST profiles for A_6-DNA revealed a dip at the chemical shift of the ss ES (Figures 3A, 3C, S5). Fitting the CEST profiles

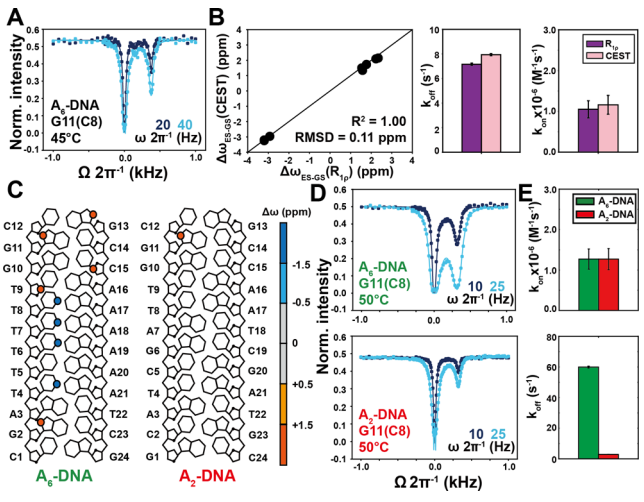

Figure 3. Site-specific characterization of hybridization kinetics using CEST. (A) ^{13}C CEST profile for G11(C8) measured in A_6-DNA at 45 °C. (B) Comparison of $\Delta\omega_{ES\text{-}GS}$, k_{off}, and k_{on} values obtained from $R_{1\rho}$ and CEST (fits of the $R_{1\rho}$ profiles were preformed fixing p_{ss} to the value measured using CEST). Buffer conditions were 25 mM NaCl, 15 mM sodium phosphate, 0.1 mM EDTA, and 10% D_2O at pH 6.8. (C) The sequence of A_2-DNA and A_6-DNA. $\Delta\omega = \omega_{ES} - \omega_{GS}$ obtained from CEST fitting is color-coded on each atom. (D) ^{13}C CEST profiles for G11(C8) measured in A_2-DNA and A_6-DNA at 50 °C. (E) Comparison of k_{on} and k_{off} values measured for A_2-DNA (red) and A_6-DNA (green).

DOI: 10.1021/jacs.9b10939
J. Am. Chem. Soc. 2019, 141, 19988−19993

allowed the reliable determination of all exchange parameters including k_{on} (Figure S4), resulting in values (Figure 3B) that are in good agreement with those previously reported values for similar DNA duplexes.[45,50]

Fixing p_{ss} to the CEST determined value, the $R_{1\rho}$ RD profiles could be satisfactorily globally fitted (Figure S5), yielding exchange parameters ($k_1 = k_{off}$, $k_{-1} = k_{on} \times [ss]$, and $\Delta\omega_{ES\text{-}GS}$) that are in excellent agreement with the CEST derived values (Figure 3B, Tables S3, S4). This mutual consistency further supports the validity of the approach. Finally, we further evaluated the CEST methodology by comparing the hybridization kinetics of A_6-DNA with another A_2-DNA duplex, which has higher stability ($T_m \sim 60$ °C and [A_2-DNA] ~ 0.8 mM) (Figure 3C, 3D). Consistent with prior studies,[47−49] the two duplexes have similar k_{on} values, but k_{off} is 20-fold faster for the less stable A_6-DNA duplex (Figure 3E).

Next, we applied the methodology to examine how m^{6}A impacts hybridization kinetics in an RNA duplex containing the most abundant m^{6}A consensus sequence (GGACU) in eukaryotic mRNA[1,2] ($T_m \sim 80$ °C and [dsGGACU] ~ 0.7 mM with Mg^{2+}). In canonical RNA duplexes, there are no contributions from Hoogsteen exchange or any other process as verified for Watson−Crick bps in a variety of sequence and structural contexts.[54] However, since m^{6}A could induce local melting of the duplex, it was important to carry out measurements on the m^{6}A residue itself. To this end, two dsGGACU duplexes were chemically synthesized containing ^{13}C2/C8 labeled m^{6}A or A near the center of the duplex (Figures 4A, S1, S6) (see methods). m^{6}A destabilized the dsGGACU duplex by ~1 kcal/mol (Table S1), consistent with prior studies.[21,22]

The CEST and $R_{1\rho}$ profiles for both unmodified and modified dsGGACU duplexes at T = 65 °C revealed a single peak/dip consistent with two-state exchange (Figures 4B, S7). However, the profiles for the modified duplex differed markedly from its unmodified counterpart (Figures 4B, S7). In both cases, global fitting of the CEST and $R_{1\rho}$ data yielded ES chemical shifts that are in excellent agreement with those measured for the isolated ss (Figures 4C, S7, S8). Fitting the CEST data revealed that m^{6}A changes k_{off} by 0.7−1.7-fold but decreases k_{on} by 4−9-fold (Figures 4D, S7). This m^{6}A induced slowdown of annealing was observed robustly with or without Mg^{2+} (Figures 4D, S7), for a different sequence derived from the hepatitis C virus (HCV)[15] (T_m~76 °C and [dsHCV] ~ 0.7 mM with Mg^{2+}) (Figures S1, S7), at a higher concentration of monovalent ions (Figure S7), and when using the $R_{1\rho}$ RD data (Figure S7).

When unpaired, the N^6-methyl group favors the *syn* conformation, while the *anti* conformation required for Watson−Crick pairing and duplex annealing is unfavorable with an estimated population of ~5%.[63] Rotation of the N^6-methyl group is likely responsible for the reduced annealing rate. Mismatches have also been shown to reduce k_{on} by up to 50-fold[27,64] through mechanisms that are not fully understood. Further studies are needed to dissect the kinetic mechanism by which m^{6}A slows the annealing rate and how this varies with position and sequence context.[64]

In conclusion, we have described an NMR strategy for site-specifically resolving duplex hybridization kinetics. The ease and throughput of these experiments can be improved in the future by using longitudinal optimized ^{1}H-CEST experiments[65] as well as other approaches for optimal data collection.[34,66] The approach can also be applied to mismatch containing

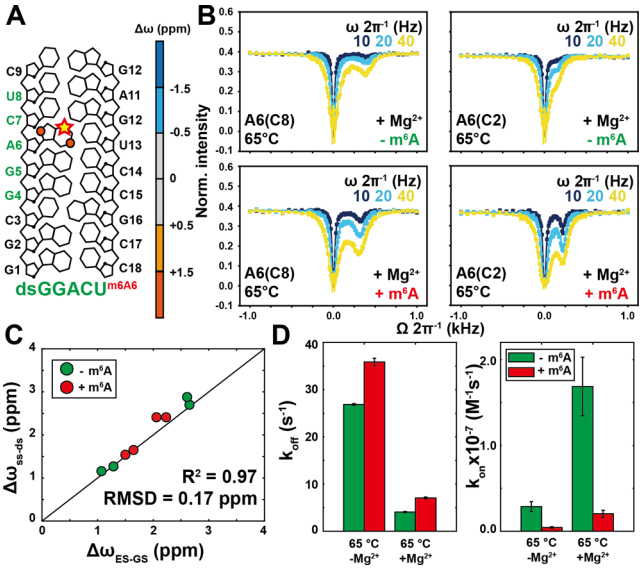

Figure 4. Measuring the impact of m^{6}A on dsGGACU hybridization kinetics using CEST. (A) The dsGGACU sequence. $\Delta\omega = \omega_{ES} - \omega_{GS}$ obtained from global fitting of CEST is color-coded on each atom. (B) ^{13}C CEST profiles measured for A6 in unmodified (left, green) and m^{6}A modified (right, red) dsGGACU at 65 °C in the presence of 3 mM Mg^{2+} (profiles in the absence of Mg^{2+} are shown in Figure S7). Buffer conditions were 25 mM NaCl, 15 mM sodium phosphate, 3 mM Mg^{2+}, 0.1 mM EDTA, and 10% D_2O at pH 6.8. (C) Comparison of $\Delta\omega_{ES\text{-}GS} = \omega_{ES} - \omega_{GS}$ measured by CEST with $\Delta\omega_{ss\text{-}ds} = \omega_{ss} - \omega_{ds}$ values obtained from the major and minor resonance observed in 2D [^{13}C,^{1}H] HSQC spectra of dsGGACU with (red) and without (green) m^{6}A at 65 °C. (D) Comparison of k_{on} and k_{off} measured for unmodified (green) and m^{6}A modified (red) dsGGACU.

duplexes ideally by targeting remote sites that are not involved in any local mismatch dynamics and to use multisite exchange models as needed to fit data.[56] Our results show that in the middle of a duplex, m^{6}A minimally affects the melting rate but substantially decreases the rate of annealing. This may help explain why tRNA selection during translation is slower for mRNAs containing m^{6}A.[20] m^{6}A is also found in the seed sequence of microRNAs and in their mRNA target sites,[67] and mismatches that slow down microRNA:mRNA annealing have substantial effects on gene expression.[64] Thus, m^{6}A could similarly affect gene expression by altering the kinetics of annealing. m^{6}A may also affect the kinetics of RNA-protein and RNA-ligand association and also reshape cotranscriptional RNA folding pathways[68−71] by prolonging the lifetime of the unpaired conformation[25,72,73] perhaps in a manner analogous to cis−trans proline isomerization in proteins.[74,75]

■ ASSOCIATED CONTENT

Supporting Information

The Supporting Information is available free of charge at https://pubs.acs.org/doi/10.1021/jacs.9b10939.

Details of sample preparation, NMR experiments, NMR $R_{1\rho}$ RD, and CEST profiles (PDF)

■ AUTHOR INFORMATION

Corresponding Authors

*hashim.al.hashimi@duke.edu

*christoph.kreutz@uibk.ac.at

DOI: 10.1021/jacs.9b10939
J. Am. Chem. Soc. 2019, 141, 19988−19993

ORCID

Honglue Shi: 0000-0003-3847-1652
Christoph Kreutz: 0000-0002-7018-9326

Author Contributions

[⊥]H.S. and B.L. contributed equally.

Notes

The authors declare the following competing financial interest(s): H.M.A. is an advisor to and holds an ownership interest in Nymirum, an RNA-based drug discovery company. The research reported in this article was performed by the Duke University faculty and students and was funded by a U.S. National Institutes of Health contract to H.M.A.

■ ACKNOWLEDGMENTS

We thank Nicole Orlovsky for critical comments on the manuscript and Prof. Lewis Kay (University of Toronto) for helpful discussions. We acknowledge the technical support and resources from the Duke Magnetic Resonance Spectroscopy Center. We thank Dr. Richard Brennan for use of the UV−vis spectrophotometer. This work was supported by US National Institute for General Medical Sciences (1R01GM132899 to H.M.A.), the Austrian Science Fund (FWF, project P28725 and P30370 to C.K.), and the Austrian Research Promotion Agency FFG (West Austrian BioNMR, 858017 to C.K.).

■ REFERENCES

(1) Meyer, K. D.; Saletore, Y.; Zumbo, P.; Elemento, O.; Mason, C. E.; Jaffrey, S. R. Comprehensive analysis of mRNA methylation reveals enrichment in 3′ UTRs and near stop codons. *Cell* **2012**, *149* (7), 1635−46.

(2) Dominissini, D.; Moshitch-Moshkovitz, S.; Schwartz, S.; Salmon-Divon, M.; Ungar, L.; Osenberg, S.; Cesarkas, K.; Jacob-Hirsch, J.; Amariglio, N.; Kupiec, M.; Sorek, R.; Rechavi, G. Topology of the human and mouse m(6)A RNA methylomes revealed by m(6)A-seq. *Nature* **2012**, *485* (7397), 201−U84.

(3) Desrosiers, R.; Friderici, K.; Rottman, F. Identification of Methylated Nucleosides in Messenger-Rna from Novikoff Hepatoma-Cells. *Proc. Natl. Acad. Sci. U. S. A.* **1974**, *71* (10), 3971−3975.

(4) Li, X.; Xiong, X.; Yi, C. Epitranscriptome sequencing technologies: decoding RNA modifications. *Nat. Methods* **2017**, *14* (1), 23−31.

(5) Wang, X.; Zhao, B. S.; Roundtree, I. A.; Lu, Z. K.; Han, D. L.; Ma, H. H.; Weng, X. C.; Chen, K.; Shi, H. L.; He, C. N-6-methyladenosine Modulates Messenger RNA Translation Efficiency. *Cell* **2015**, *161* (6), 1388−1399.

(6) Wang, X.; Lu, Z. K.; Gomez, A.; Hon, G. C.; Yue, Y. N.; Han, D. L.; Fu, Y.; Parisien, M.; Dai, Q.; Jia, G. F.; Ren, B.; Pan, T.; He, C. N-6-methyladenosine-dependent regulation of messenger RNA stability. *Nature* **2014**, *505* (7481), 117−120.

(7) Zhao, X.; Yang, Y.; Sun, B. F.; Shi, Y.; Yang, X.; Xiao, W.; Hao, Y. J.; Ping, X. L.; Chen, Y. S.; Wang, W. J.; Jin, K. X.; Wang, X.; Huang, C. M.; Fu, Y.; Ge, X. M.; Song, S. H.; Jeong, H. S.; Yanagisawa, H.; Niu, Y. M.; Jia, G. F.; Wu, W.; Tong, W. M.; Okamoto, A.; He, C.; Danielsen, J. M. R.; Wang, X. J.; Yang, Y. G. FTO-dependent demethylation of N6-methyladenosine regulates mRNA splicing and is required for adipogenesis. *Cell Res.* **2014**, *24* (12), 1403−1419.

(8) Xiao, W.; Adhikari, S.; Dahal, U.; Chen, Y. S.; Hao, Y. J.; Sun, B. F.; Sun, H. Y.; Li, A.; Ping, X. L.; Lai, W. Y.; Wang, X.; Ma, H. L.; Huang, C. M.; Yang, Y.; Huang, N.; Jiang, G. B.; Wang, H. L.; Zhou, Q.; Wang, X. J.; Zhao, Y. L.; Yang, Y. G. Nuclear m(6)A Reader YTHDC1 Regulates mRNA Splicing. *Mol. Cell* **2016**, *61* (4), 507−519.

(9) Zhao, B. X. S.; Roundtree, I. A.; He, C. Post-transcriptional gene regulation by mRNA modifications. *Nat. Rev. Mol. Cell Biol.* **2017**, *18* (1), 31−42.

(10) Roundtree, I. A.; Evans, M. E.; Pan, T.; He, C. Dynamic RNA Modifications in Gene Expression Regulation. *Cell* **2017**, *169* (7), 1187−1200.

(11) Meyer, K. D.; Jaffrey, S. R. Rethinking m(6)A Readers, Writers, and Erasers. *Annu. Rev. Cell Dev. Biol.* **2017**, *33*, 319−342.

(12) Deng, X. L.; Su, R.; Feng, X. S.; Wei, M. J.; Chen, J. J. Role of N-6-methyladenosine modification in cancer. *Curr. Opin. Genet. Dev.* **2018**, *48*, 1−7.

(13) Chen, T.; Hao, Y.-J.; Zhang, Y.; Li, M.-M.; Wang, M.; Han, W.; Wu, Y.; Lv, Y.; Hao, J.; Wang, L.; Li, A.; Yang, Y.; Jin, K.-X.; Zhao, X.; Li, Y.; Ping, X.-L.; Lai, W.-Y.; Wu, L.-G.; Jiang, G.; Wang, H.-L.; Sang, L.; Wang, X.-J.; Yang, Y.-G.; Zhou, Q. m6A RNA Methylation Is Regulated by MicroRNAs and Promotes Reprogramming to Pluripotency. *Cell stem cell* **2015**, *16* (3), 289−301.

(14) Weng, Y.-L.; Wang, X.; An, R.; Cassin, J.; Vissers, C.; Liu, Y.; Liu, Y.; Xu, T.; Wang, X.; Wong, S. Z. H.; Joseph, J.; Dore, L. C.; Dong, Q.; Zheng, W.; Jin, P.; Wu, H.; Shen, B.; Zhuang, X.; He, C.; Liu, K.; Song, H.; Ming, G.-l. Epitranscriptomic m6A Regulation of Axon Regeneration in the Adult Mammalian Nervous System. *Neuron* **2018**, *97* (2), 313−325.e6.

(15) Gokhale, N. S.; McIntyre, A. B. R.; McFadden, M. J.; Roder, A. E.; Kennedy, E. M.; Gandara, J. A.; Hopcraft, S. E.; Quicke, K. M.; Vazquez, C.; Willer, J.; Ilkayeva, O. R.; Law, B. A.; Holley, C. L.; Garcia-Blanco, M. A.; Evans, M. J.; Suthar, M. S.; Bradrick, S. S.; Mason, C. E.; Horner, S. M. N6-Methyladenosine in Flaviviridae Viral RNA Genomes Regulates Infection. *Cell Host Microbe* **2016**, *20* (5), 654−665.

(16) Liu, N.; Dai, Q.; Zheng, G.; He, C.; Parisien, M.; Pan, T. N6-methyladenosine-dependent RNA structural switches regulate RNA−protein interactions. *Nature* **2015**, *518*, 560.

(17) Huang, L.; Ashraf, S.; Wang, J.; Lilley, D. M. J. Control of box C/D snoRNP assembly by N(6)-methylation of adenine. *EMBO Rep.* **2017**, *18* (9), 1631.

(18) Spitale, R. C.; Flynn, R. A.; Zhang, Q. C.; Crisalli, P.; Lee, B.; Jung, J.-W.; Kuchelmeister, H. Y.; Batista, P. J.; Torre, E. A.; Kool, E. T.; Chang, H. Y. Structural imprints in vivo decode RNA regulatory mechanisms. *Nature* **2015**, *519*, 486.

(19) Liu, B.; Merriman, D. K.; Choi, S. H.; Schumacher, M. A.; Plangger, R.; Kreutz, C.; Horner, S. M.; Meyer, K. D.; Al-Hashimi, H. M. A potentially abundant junctional RNA motif stabilized by m(6)A and Mg(2). *Nat. Commun.* **2018**, *9* (1), 2761.

(20) Choi, J.; Ieong, K.-W.; Demirci, H.; Chen, J.; Petrov, A.; Prabhakar, A.; O'Leary, S. E.; Dominissini, D.; Rechavi, G.; Soltis, S. M.; Ehrenberg, M.; Puglisi, J. D. N6-methyladenosine in mRNA disrupts tRNA selection and translation-elongation dynamics. *Nat. Struct. Mol. Biol.* **2016**, *23*, 110.

(21) Roost, C.; Lynch, S. R.; Batista, P. J.; Qu, K.; Chang, H. Y.; Kool, E. T. Structure and Thermodynamics of N6-Methyladenosine in RNA: A Spring-Loaded Base Modification. *J. Am. Chem. Soc.* **2015**, *137* (5), 2107−2115.

(22) Kierzek, E.; Kierzek, R. The thermodynamic stability of RNA duplexes and hairpins containing N-6-alkyladenosines and 2-methylthio-N-6-alkyladenosines. *Nucleic Acids Res.* **2003**, *31* (15), 4472−4480.

(23) Dethoff, E. A.; Petzold, K.; Chugh, J.; Casiano-Negroni, A.; Al-Hashimi, H. M. Visualizing transient low-populated structures of RNA. *Nature* **2012**, *491* (7426), 724−8.

(24) Ganser, L. R.; Kelly, M. L.; Herschlag, D.; Al-Hashimi, H. M. The roles of structural dynamics in the cellular functions of RNAs. *Nat. Rev. Mol. Cell Biol.* **2019**, *20* (8), 474−489.

(25) Steinert, H.; Sochor, F.; Wacker, A.; Buck, J.; Helmling, C.; Hiller, F.; Keyhani, S.; Noeske, J.; Grimm, S.; Rudolph, M. M.; Keller, H.; Mooney, R. A.; Landick, R.; Suess, B.; Furtig, B.; Wohnert, J.; Schwalbe, H. Pausing guides RNA folding to populate transiently stable RNA structures for riboswitch-based transcription regulation. *eLife* **2017**, *6*, e21297.

(26) Becker, W. R.; Ober-Reynolds, B.; Jouravleva, K.; Jolly, S. M.; Zamore, P. D.; Greenleaf, W. J. High-Throughput Analysis Reveals

DOI: 10.1021/jacs.9b10939
J. Am. Chem. Soc. 2019, 141, 19988−19993

Rules for Target RNA Binding and Cleavage by AGO2. *Mol. Cell* **2019**, *75* (4), 741−755.e11.
(27) Cisse, I. I.; Kim, H.; Ha, T. A rule of seven in Watson-Crick base-pairing of mismatched sequences. *Nat. Struct. Mol. Biol.* **2012**, *19* (6), 623−627.
(28) Gleitsman, K. R.; Sengupta, R. N.; Herschlag, D. Slow molecular recognition by RNA. *RNA* **2017**, *23* (12), 1745−1753.
(29) Larsen, K. P.; Choi, J.; Prabhakar, A.; Puglisi, E. V.; Puglisi, J. D. Relating Structure and Dynamics in RNA Biology. *Cold Spring Harbor Perspect. Biol.* **2019**, *11* (7), a032474.
(30) Massi, F.; Johnson, E.; Wang, C. Y.; Rance, M.; Palmer, A. G. NMR R-1 rho rotating-frame relaxation with weak radio frequency fields. *J. Am. Chem. Soc.* **2004**, *126* (7), 2247−2256.
(31) Rangadurai, A.; Szymaski, E. S.; Kimsey, I. J.; Shi, H.; Al-Hashimi, H. M. Characterizing micro-to-millisecond chemical exchange in nucleic acids using off-resonance R1ρ relaxation dispersion. *Prog. Nucl. Magn. Reson. Spectrosc.* **2019**, *112*−*113*, 55−102.
(32) Palmer, A. G.; Massi, F. Characterization of the dynamics of biomacromolecules using rotating-frame spin relaxation NMR spectroscopy. *Chem. Rev.* **2006**, *106* (5), 1700−1719.
(33) Zhao, B.; Hansen, A. L.; Zhang, Q. Characterizing slow chemical exchange in nucleic acids by carbon CEST and low spin-lock field R(1rho) NMR spectroscopy. *J. Am. Chem. Soc.* **2014**, *136* (1), 20−3.
(34) Vallurupalli, P.; Bouvignies, G.; Kay, L. E. Studying "invisible" excited protein states in slow exchange with a major state conformation. *J. Am. Chem. Soc.* **2012**, *134* (19), 8148−61.
(35) Steitz, J. RNA-RNA base-pairing: theme and variations. *RNA* **2015**, *21* (4), 476−7.
(36) Jung, J.; Van Orden, A. Folding and Unfolding Kinetics of DNA Hairpins in Flowing Solution by Multiparameter Fluorescence Correlation Spectroscopy. *J. Phys. Chem. B* **2005**, *109* (8), 3648−3657.
(37) Jung, J.; Van Orden, A. A Three-State Mechanism for DNA Hairpin Folding Characterized by Multiparameter Fluorescence Fluctuation Spectroscopy. *J. Am. Chem. Soc.* **2006**, *128* (4), 1240−1249.
(38) Chen, X. D.; Zhou, Y.; Qu, P.; Zhao, X. S. Base-by-Base Dynamics in DNA Hybridization Probed by Fluorescence Correlation Spectroscopy. *J. Am. Chem. Soc.* **2008**, *130* (50), 16947−16952.
(39) Nayak, R. K.; Peersen, O. B.; Hall, K. B.; Van Orden, A. Millisecond Time-Scale Folding and Unfolding of DNA Hairpins Using Rapid-Mixing Stopped-Flow Kinetics. *J. Am. Chem. Soc.* **2012**, *134* (5), 2453−2456.
(40) He, G.; Li, J.; Ci, H. N.; Qi, C. M.; Guo, X. F. Direct Measurement of Single-Molecule DNA Hybridization Dynamics with Single-Base Resolution. *Angew. Chem., Int. Ed.* **2016**, *55* (31), 9036−9040.
(41) Wetmur, J. G.; Davidson, N. Kinetics of Renaturation of DNA. *J. Mol. Biol.* **1968**, *31* (3), 349−370.
(42) Wetmur, J. G. Hybridization and Renaturation Kinetics of Nucleic-Acids. *Annu. Rev. Biophys. Bioeng.* **1976**, *5*, 337−361.
(43) Bonnet, G.; Krichevsky, O.; Libchaber, A. Kinetics of conformational fluctuations in DNA hairpin-loops. *Proc. Natl. Acad. Sci. U. S. A.* **1998**, *95* (15), 8602−8606.
(44) Williams, A. P.; Longfellow, C. E.; Freier, S. M.; Kierzek, R.; Turner, D. H. Laser Temperature-Jump, Spectroscopic, and Thermodynamic Study of Salt Effects on Duplex Formation by Dgcatgc. *Biochemistry* **1989**, *28* (10), 4283−4291.
(45) Howorka, S.; Movileanu, L.; Braha, O.; Bayley, H. Kinetics of duplex formation for individual DNA strands within a single protein nanopore. *Proc. Natl. Acad. Sci. U. S. A.* **2001**, *98* (23), 12996−3001.
(46) Kimsey, I. J.; Szymanski, E. S.; Zahurancik, W. J.; Shakya, A.; Xue, Y.; Chu, C. C.; Sathyamoorthy, B.; Suo, Z. C.; Al-Hashimi, H. M. Dynamic basis for dG.dT misincorporation via tautomerization and ionization. *Nature* **2018**, *554* (7691), 195−201.
(47) Rauzan, B.; McMichael, E.; Cave, R.; Sevcik, L. R.; Ostrosky, K.; Whitman, E.; Stegemann, R.; Sinclair, A. L.; Serra, M. J.; Deckert, A. A. Kinetics and Thermodynamics of DNA, RNA, and Hybrid Duplex Formation. *Biochemistry* **2013**, *52* (5), 765−772.
(48) Craig, M. E.; Crothers, D. M.; Doty, P. Relaxation Kinetics of Dimer Formation by Self Complementary Oligonucleotides. *J. Mol. Biol.* **1971**, *62* (2), 383−401.
(49) Pörschke, D.; Uhlenbeck, O. C.; Martin, F. H. Thermodynamics and kinetics of the helix-coil transition of oligomers containing GC base pairs. *Biopolymers* **1973**, *12* (6), 1313−1335.
(50) Wyer, J. A.; Kristensen, M. B.; Jones, N. C.; Hoffmann, S. V.; Nielsen, S. B. Kinetics of DNA duplex formation: A-tracts versus AT-tracts. *Phys. Chem. Chem. Phys.* **2014**, *16* (35), 18827−39.
(51) Braunlin, W. H.; Bloomfield, V. A. H-1-Nmr Study of the Base-Pairing Reactions of D(Ggaattcc) - Salt Effects on the Equilibria and Kinetics of Strand Association. *Biochemistry* **1991**, *30* (3), 754−758.
(52) Mulder, F. A.; Mittermaier, A.; Hon, B.; Dahlquist, F. W.; Kay, L. E. Studying excited states of proteins by NMR spectroscopy. *Nat. Struct. Biol.* **2001**, *8* (11), 932−5.
(53) Xue, Y.; Kellogg, D.; Kimsey, I. J.; Sathyamoorthy, B.; Stein, Z. W.; McBrairty, M.; Al-Hashimi, H. M. Characterizing RNA Excited States Using NMR Relaxation Dispersion. *Methods Enzymol.* **2015**, *558*, 39−73.
(54) Zhou, H.; Kimsey, I. J.; Nikolova, E. N.; Sathyamoorthy, B.; Grazioli, G.; McSally, J.; Bai, T.; Wunderlich, C. H.; Kreutz, C.; Andricioaei, I.; Al-Hashimi, H. M. m1A and m1G disrupt A-RNA structure through the intrinsic instability of Hoogsteen base pairs. *Nat. Struct. Mol. Biol.* **2016**, *23* (9), 803−810.
(55) Nikolova, E. N.; Kim, E.; Wise, A. A.; O'Brien, P. J.; Andricioaei, I.; Al-Hashimi, H. M. Transient Hoogsteen base pairs in canonical duplex DNA. *Nature* **2011**, *470* (7335), 498−502.
(56) Kimsey, I. J.; Petzold, K.; Sathyamoorthy, B.; Stein, Z. W.; Al-Hashimi, H. M. Visualizing transient Watson-Crick-like mispairs in DNA and RNA duplexes. *Nature* **2015**, *519* (7543), 315−20.
(57) Sathyamoorthy, B.; Shi, H.; Zhou, H.; Xue, Y.; Rangadurai, A.; Merriman, D. K.; Al-Hashimi, H. M. Insights into Watson−Crick/Hoogsteen breathing dynamics and damage repair from the solution structure and dynamic ensemble of DNA duplexes containing m1A. *Nucleic Acids Res.* **2017**, *45* (9), 5586−5601.
(58) Shi, H.; Clay, M. C.; Rangadurai, A.; Sathyamoorthy, B.; Case, D. A.; Al-Hashimi, H. M. Atomic structures of excited state A−T Hoogsteen base pairs in duplex DNA by combining NMR relaxation dispersion, mutagenesis, and chemical shift calculations. *J. Biomol. NMR* **2018**, *70* (4), 229−244.
(59) Alvey, H. S.; Gottardo, F. L.; Nikolova, E. N.; Al-Hashimi, H. M. Widespread transient Hoogsteen base pairs in canonical duplex DNA with variable energetics. *Nat. Commun.* **2014**, *5*, 4786.
(60) Pörschke, D.; Eigen, M. Co-operative non-enzymatic base recognition III. Kinetics of the helix—coil transition of the oligoribouridylic · oligoriboadenylic acid system and of oligoriboadenylic acid alone at acidic pH. *J. Mol. Biol.* **1971**, *62* (2), 361−381.
(61) Vallurupalli, P.; Sekhar, A.; Yuwen, T. R.; Kay, L. E. Probing conformational dynamics in biomolecules via chemical exchange saturation transfer: a primer. *J. Biomol. NMR* **2017**, *67* (4), 243−271.
(62) Bouvignies, G.; Hansen, D. F.; Vallurupalli, P.; Kay, L. E. Divided-Evolution-Based Pulse Scheme for Quantifying Exchange Processes in Proteins: Powerful Complement to Relaxation Dispersion Experiments. *J. Am. Chem. Soc.* **2011**, *133* (6), 1935−1945.
(63) Engel, J. D.; Von Hippel, P. H. Effects of methylation on the stability of nucleic acid conformations. Monomer level. *Biochemistry* **1974**, *13* (20), 4143−4158.
(64) Miller, C. L.; Haas, U.; Diaz, R.; Leeper, N. J.; Kundu, R. K.; Patlolla, B.; Assimes, T. L.; Kaiser, F. J.; Perisic, L.; Hedin, U.; Maegdefessel, L.; Schunkert, H.; Erdmann, J.; Quertermous, T.; Sczakiel, G. Coronary heart disease-associated variation in TCF21 disrupts a miR-224 binding site and miRNA-mediated regulation. *PLoS Genet.* **2014**, *10* (3), No. e1004263.
(65) Yuwen, T.; Kay, L. E. Longitudinal relaxation optimized amide (1)H-CEST experiments for studying slow chemical exchange

DOI: 10.1021/jacs.9b10939
J. Am. Chem. Soc. 2019, 141, 19988−19993

processes in fully protonated proteins. *J. Biomol. NMR* **2017**, *67* (4), 295−307.
(66) Bouvignies, G.; Kay, L. E. A 2D C-13-CEST experiment for studying slowly exchanging protein systems using methyl probes: an application to protein folding. *J. Biomol. NMR* **2012**, *53* (4), 303−310.
(67) Linder, B.; Grozhik, A. V.; Olarerin-George, A. O.; Meydan, C.; Mason, C. E.; Jaffrey, S. R. Single-nucleotide-resolution mapping of m6A and m6Am throughout the transcriptome. *Nat. Methods* **2015**, *12* (8), 767−72.
(68) Heilman-Miller, S. L.; Woodson, S. A. Effect of transcription on folding of the Tetrahymena ribozyme. *RNA* **2003**, *9* (6), 722−33.
(69) Kramer, F. R.; Mills, D. R. Secondary structure formation during RNA synthesis. *Nucleic Acids Res.* **1981**, *9* (19), 5109−24.
(70) Pan, T.; Artsimovitch, I.; Fang, X. W.; Landick, R.; Sosnick, T. R. Folding of a large ribozyme during transcription and the effect of the elongation factor NusA. *Proc. Natl. Acad. Sci. U. S. A.* **1999**, *96* (17), 9545−50.
(71) Wong, T. N.; Sosnick, T. R.; Pan, T. Folding of noncoding RNAs during transcription facilitated by pausing-induced nonnative structures. *Proc. Natl. Acad. Sci. U. S. A.* **2007**, *104* (46), 17995−8000.
(72) Zhao, B.; Guffy, S. L.; Williams, B.; Zhang, Q. An excited state underlies gene regulation of a transcriptional riboswitch. *Nat. Chem. Biol.* **2017**, *13* (9), 968−974.
(73) Breaker, R. R. Riboswitches and Translation Control. *Cold Spring Harbor Perspect. Biol.* **2018**, *10* (11), a032797.
(74) Brandts, J. F.; Halvorson, H. R.; Brennan, M. Consideration of the possibility that the slow step in protein denaturation reactions is due to cis-trans isomerism of proline residues. *Biochemistry* **1975**, *14* (22), 4953−4963.
(75) Wedemeyer, W. J.; Welker, E.; Scheraga, H. A. Proline cis-trans isomerization and protein folding. *Biochemistry* **2002**, *41* (50), 14637−14644.

DOI: 10.1021/jacs.9b10939
J. Am. Chem. Soc. 2019, 141, 19988−19993